HHS Public Access

Author manuscript

Structure. Author manuscript; available in PMC 2016 July 07.

Published in final edited form as:

Structure. 2015 July 7; 23(7): 1258–1270. doi:10.1016/j.str.2015.04.020.

Structure of dimeric and tetrameric complexes of the BAR domain protein PICK1 determined by small-angle X-ray scattering

Morten L. Karlsen[#1], **Thor S. Thorsen**[#1], **Niklaus Johner**[5], **Ina Ammendrup-Johnsen**[1], **Simon Erlendsson**[1,3], **Xinsheng Tian**[4], **Jens B. Simonsen**[2], **Rasmus Høiberg-Nielsen**[2], **Nikolaj M. Christensen**, **George Khelashvili**[5], **Werner Streicher**[6], **Kaare Teilum**[3], **Bente Vestergaard**[4], **Harel Weinstein**[5], **Ulrik Gether**[1], **Lise Arleth**[2,**], and **Kenneth L. Madsen**[1,**]

[1]Molecular Neuropharmacology and Genetics Laboratory, Lundbeck Foundation Center for Biomembranes in Nanomedicine, Department of Neuroscience and Pharmacology, Faculty of Health and Medical Sciences, The Panum Institute 18.6, University of Copenhagen, 2200 Copenhagen N, Denmark.

[2]Structural Biophysics, Niels Bohr Institute, University of Copenhagen, Universitetsparken 5, 2100 Copenhagen Ø, Denmark

[3]Structural Biology and NMR Laboratory, Department of Biology, Faculty of Science, University of Copenhagen, Ole Maaløes Vej 5, 2200 Copenhagen N, Denmark.

[4]Biostructural Research, Department of Drug Design and Pharmacology, University of Copenhagen, Universitetsparken 2, 2100 Copenhagen Ø, Denmark

[5]Department of Physiology and Biophysics, Weill Cornell Medical College, Cornell University, Room E-509, 1300 York Avenue, 10065, New York City, NY, USA

[6]NNF Center for Protein Research, Faculty of Health and Medical Sciences, University of Copenhagen, Blegdamsvej 3, 2200 Copenhagen N, Denmark.

[#] These authors contributed equally to this work.

Summary

PICK1 is a neuronal scaffolding protein containing a PDZ domain and an autoinhibited BAR domain. BAR domains are membrane-sculpting protein modules generating membrane curvature and promoting membrane fission. Previous data suggest that BAR domains are organized in lattice-like arrangements when stabilizing membranes but little is known about structural organization of BAR domains in solution. Through a small-angle X-ray scattering (SAXS) analysis, we determine the structure of dimeric and tetrameric complexes of PICK1 in solution.

[**] Correspondence: kennethma@sund.ku.dk/arleth@nbi.ku.dk.
Current address: Novozymes A/S, DK-2880 Bagsværd, Denmark

Author Contributions

TT purified, characterized and prepared protein for SAXS. MLK performed and developed SAXS analysis.

SAXS and biochemical data reveal a strong propensity of PICK1 to form higher order structures and SAXS analysis suggest an offset, parallel mode of BAR-BAR oligomerization. Furthermore, unlike accessory domains in other BAR domain proteins, the positioning of the PDZ domains is flexible, enabling PICK1 to perform long-range, dynamic scaffolding of membrane-associated proteins. Together with functional data, these structural findings are compatible with a model where oligomerization governs auto-inhibition of BAR domain function.

Introduction

PICK1 (Protein Interacting with C Kinase) is a scaffolding protein localized to neurons as well as to muscle and endocrine cells (Cao et al., 2007; Jansen et al., 2009; Staudinger et al., 1995). The protein serves distinct roles in scaffolding of kinases (Perez et al., 2001; Staudinger et al., 1997), direct modulation of membrane protein function (Sogaard et al., 2013), regulation of membrane protein trafficking (Citri et al., 2010; Madsen et al., 2012) and membrane remodeling during biogenesis of dense core vesicles (Cao et al., 2013; Holst et al., 2013). At the N-terminus, PICK1 harbors a PSD-95/Discs-Large/ZO-1 homology (PDZ) domain that mediates protein-protein interactions with a number of transmembrane proteins including receptors, ion channels and transporters, as well as with PKC α (Xu and Xia, 2006). A central Bin/amphiphysin/Rvs (BAR) domain facilitates PICK1 dimerization, which is important for both its scaffolding function of PICK1 and for its ability to bind to and remodel the cell membrane (Citri et al., 2010; Jin et al., 2006; Lu and Ziff, 2005; Madsen et al., 2012).

PICK1 is central in regulating trafficking of AMPA-type glutamate receptors (AMPARs) during synaptic plasticity. PICK1 binds the intracellular C-terminus of the AMPAR subunit GluA2 (Xia et al., 1999) and regulates its plasma membrane localization in an activity dependent manner (Anggono and Huganir, 2012). This function, as well as the synaptic localization of PICK1, depends on the membrane binding BAR domain (Jin et al., 2006; Steinberg et al., 2006). Similar to endophilin and the F-BAR protein syndapin-1 (Meinecke et al., 2013; Rao et al., 2010), the membrane and protein binding function of the PICK1 BAR domain is auto-inhibited (Jin et al., 2006; Lu and Ziff, 2005; Madsen et al., 2008; Rocca et al., 2008). This auto-inhibition of the PICK1 BAR domain is believed to involve the N-terminal PDZ domain (Lu and Ziff, 2005; Madsen et al., 2008) and as well as the unstructured C-terminus (Jin et al., 2006). A steric hindrance model suggesting direct interaction of the PDZ and BAR domains has been proposed for the PICK1 auto-inhibition (Hanley, 2008; Lu and Ziff, 2005).

For both endophilin and syndapin, auto-inhibition is relieved by dynamin binding to the SH3 domain (Meinecke et al., 2013; Rao et al., 2010) and similarly peptide binding in the PDZ domain was suggested to relieve PICK1 auto-inhibition (Lu and Ziff, 2005; Rocca et al., 2008). In addition, Ca^{2+}-binding was proposed to regulate the auto-inhibition (Citri et al., 2010), whereas our previous work suggests that membrane recruitment is key to BAR domain activation (Madsen et al., 2008).

Crystal structures of numerous BAR domains have been solved, but only few studies have provided insight into the structural organization of individual domains relative to one

another in full-length BAR domain proteins. For sorting nexin 9 (Snx9), endophilin, APPL1 and syndapin-1, their respective accessory domains were all associated with either the side or the tip of the BAR domain (Li et al., 2007; Pylypenko et al., 2007; Rao et al., 2010; Wang et al., 2008; Zhu et al., 2007). To investigate the structural interdomain arrangement in PICK1, which is believed to underlie the auto-inhibition mechanism, we engaged in small-angle X-ray scattering (SAXS) studies of full-length PICK1 in solution. We demonstrate that PICK1 is highly prone to oligomerization, even in absence of lipid membrane, and we obtain the first solution based structural information of BAR domain oligomerization using rigid body modelling in combination with Ensemble Optimization Method (EOM) analysis. The data suggest an elongated tetrameric conformation with individual dimers overlapping along one third of the length of the dimer - i.e. an elongated, overlapping mode of BAR-BAR oligomerization. Using a non-oligomerizing mutant of PICK1, together with a novel method for analytical decomposition of the scattering data followed by EOM, we furthermore show that the PDZ domains are flexible and far apart and consequently enable PICK1 to perform highly flexible, long range scaffolding of membrane associated protein complexes.

Results

Biochemical characterization of PICK1^{WT} and PICK1^{LKV}

Wild type PICK1 (PICK1^{WT}) was expressed in *E. Coli* and purified as described (Madsen et al., 2005). The size of purified PICK1^{WT} was verified by SDS-PAGE (Figure 1A) and subsequently evaluated by size exclusion chromatography (SEC) revealing two peaks for PICK1^{WT}. The early peak, eluting at ~8.5 ml (peak 1), most likely represented large oligomeric states (Figure 1B). These large oligomers were almost completely removed by ultracentrifugation (Figure 1B, dashed). The main peak (peak 2, ~12 ml) was composed of at least two overlapping peaks presumably representing the dimeric form of PICK1^{WT} as well as higher order oligomeric forms (Figure 1B, dashed). This suggests very little monomeric protein in our samples. To test whether we could indeed detect the monomer, we increased the Triton X-100 (TX-100) concentration to 0.1%. Under these conditions the main peak eluted later (~13 ml), suggesting separation into monomers (Figure S1A). This was further substantiated by crosslinking experiments (Figure S1B). Analytical ultra-centrifugation (AUC) of peak 2 obtained in 0.01% TX-100 supported PICK1 oligomerization by revealing several species (Figure 1C), likely corresponding to dimers (~3S [Svedberg], b)), tetramers (~4S, c) and octamers (~7S, e), as well as a featureless signal at high S representing even higher order oligomers. Moreover, a small peak was seen (~1S), that might be the degradation product seen as a faint band on the SDS-PAGE (Figure 1A).

We also investigated the oligomeric status of PICK1 in living cells. COS-7 cells transfected with PICK1^{WT} (N-terminal *cmyc*-tag) were treated with the cell permeable crosslinking agent disuccinimidyl suberate (DSS, 1 mM). Western blotting of the cell lysates revealed that crosslinking not only increased the dimeric fraction (100 kD), but also produced several distinct larger species suggesting the presence of dimers and higher order oligomers in living cells as well (Figure 1D).

The PICK1 PDZ domain alone has previously been stabilized for structural studies by fusion of a C-terminal sequence that docks into the peptide binding groove in the PDZ domain (Elkins et al., 2007). Using a similar approach for the full-length protein, we substituted the three C-terminal residues of PICK1 with the three C-terminal residues of the dopamine transporter - the minimal binding sequence of the PICK1 PDZ domain (CDS->LKV; PICK1$^{LKV)}$). Purified PICK1^{LKV} remained stable without precipitating at high concentrations (data not shown) and no degradation was visible on SDS-PAGE (Figure 1A). Interestingly, SEC of purified PICK1^{LKV} showed almost no higher order oligomers or aggregates (peak 1) (Figure 1B). In addition, the second peak (peak 2) was more distinct and almost without the shoulder seen for PICK1^{WT} (Figure 1B). AUC of peak 2 from the SEC revealed a more distinct peak and a larger fraction of dimer (~3S) than seen for PICK1^{WT} (Figure 1C). Consistently, the tetrameric peak (~4S) (c) was markedly reduced compared to that of PICK1^{WT} and at higher S values we only observed two very shallow peaks (Figure 1C). We did not observe the small peak (~1S) for PICK1^{LKV}, in agreement with the lack of degradation on the SDS-PAGE (Figure 1C). In conclusion, PICK1^{LKV} appeared more stable and had lower tendency to form higher order oligomers and aggregates as compared to PICK1^{WT}.

PICK1^{LKV} alleviates the auto-inhibition of PICK1

Next, we expressed YFP-PICK1^{WT} and -PICK1^{LKV} in COS7 cells. Confocal microscopy showed diffuse localization of YFP-PICK1^{WT} throughout the cytosol albeit with numerous weak clusters of the protein (Figure 1E). This partial clustering was previously suggested to reflect the membrane binding capacity of the protein (Jin et al., 2006). Somewhat counterintuitively in light of the biochemical data, YFP-PICK1^{LKV} demonstrated massive clustering indicating stronger membrane binding capacity (Figure 1E). One possible explanation could be that the auto-inhibition of the BAR domain was alleviated in YFP-PICK1^{LKV}.

To address this in more detail, we tested the membrane vesiculation capacity of PICK1^{WT} and PICK1^{LKV} by adopting a modified version of a vesiculation assay that recently was used to demonstrate a critical role in membrane scission of amphipathic helices in the N-BAR proteins endophilin A1 and amphiphysin (Boucrot et al., 2012). Indeed, our previous data have indicated that an amphipathic helix adjacent to the BAR domain is critical for the membrane-deforming capacity of PICK1 (Holst et al., 2013). The assay is based on the ability of N-BAR domains to promote formation of nanovesicles by scission/fission when incubated with liposomes. If formed, the nanovesicles will be present in the supernatant after ultracentrifugation in contrast to the liposomes that will be present in the pellet (Boucrot et al., 2012). We incubated fluorescently labeled liposomes with or without purified PICK1^{WT}, PICK1^{LKV} or endophilin1A followed by ultra-centrifugation. Consistent with the ability of endophilin1A to promote formation of nanovesicles, endophilin markedly increased fluorescence in the supernatant compared to control (no protein added) (Figure 1F). PICK1^{WT} also increased fluorescence and the increase was significantly higher for PICK1^{LKV} (Figure 1F). This demonstrates the membrane vesiculation capacity of PICK1 and further supports that the auto-inhibition of the PICK1 BAR domain is at least partially alleviated in PICK1^{LKV}.

SAXS analysis of PICK1^{WT} and PICK1^{LKV} - Visual inspection

SAXS profiles of ultra-centrifuged PICK1^{WT} and PICK1^{LKV} both showed a monotonously decaying scattering intensity as a function of the scattering vector *q* (Figure 2A, B). In both systems the forward scattering, *I(0)*, of the concentration normalized data increases with concentration (Figure 2A and 2B, see insets). This is a clear indication of a concentration-dependent oligomerization (see table in Figure 2). The effect was more pronounced for PICK1^{WT} than for PICK1^{LKV}.

The pair distance distribution functions, *p(r)*, functions for PICK1^{WT} (Figure 2C) and PICK1^{LKV} (Figure 2D), calculated by indirect Fourier transformation (IFT) (Glatter., 1977; Pedersen et al., 1994), all revealed skewed shapes with a prominent tail at large distances, akin to the *p(r)*'s previously found for endophilin and Snx9 (Wang et al., 2008), and consistent with an overall elongated shape. The D_{max} and R_g values also exhibited a concentration-dependent increase consistent with that observed in the *I(0)*-data and showed that, at similar concentrations, larger structures are formed by PICK1^{WT} than by PICK1^{LKV} (see table in Figure 2).

Neither calcium nor peptide binding induce significant conformational changes in PICK1

Ca^{2+} or PDZ ligand binding was previously suggested to regulate auto-inhibition of the PICK1 BAR domain (Citri et al., 2010; Lu and Ziff, 2005; Rocca et al., 2008). SAXS data and *p(r)* functions for PICK1^{WT} in absence and presence of 50 μM free Ca^{2+}, 100 μM GluA2 or both, showed no significant differences (Figure S2), strongly suggesting no significant change in tertiary or quaternary structure upon binding of Ca^{2+} and/or GluA2 PDZ-ligand. This is in agreement with our previous findings that peptide binding did not increase lipid binding and neither peptide binding or Ca^{2+} were sufficient to induce cellular clustering (Madsen et al., 2008).

Decomposition of the PICK1^{LKV} SAXS signal into dimer and tetramer form factors

With the concentration-induced oligomerization of the samples it was clear that each sample contained more than one structural species. To circumvent this problem, the PICK1^{LKV} SAXS data were decomposed into their underlying dimeric and tetrameric form factors by combining data from samples with different protein concentrations and hence different dimer/tretamer ratios. This was done through an approach that is a special case of singular value decomposition that assumes that only two species are present in the sample (details in SI). Assuming that the four PICK1^{LKV} samples only contained dimers and tetramers, the four PICK1^{LKV} SAXS data-set were combined in six different ways providing six different versions of the decomposed dimer and tetramer form factors (Figure 3). Direct comparison of the form factors and their *p(r)* functions (Figure 3B, C) revealed a sufficiently strong similarity between the results obtained by different combinations to implicitly validate the decomposition method and its preassumption of only two species in the case of PICK1^{LKV}. The final average PICK1^{LKV} dimer and tetramer form factors and *p(r)*'s are plotted in Figure 3D. For the PICK1^{LKV} dimer, D_{max} was consistently 200 Å and R_g was 61 +/−1 Å. This is slightly larger than reported values for the related BAR domain proteins Snx9$^{full\text{-}length}$ (D_{max} 172.5 Å, R_g 51.7 +/− 0.5 Å) and endophilin$^{full\text{-}length}$ (D_{max} 167.5 Å, R_g 48.0 +/− 0.5 Å) (Wang et al., 2008). The tetramer form factor was slightly less well defined and gave a D_{max}

of ~250 Å and an R_g of 75 +/− 3 Å. In the PICK1^{WT} system, a similar decomposition was not possible due to the presence of higher order oligomeric species.

Definition of structural modules composing PICK1

To enable rigid body modelling the structure of the individual protein domains was defined. For the PDZ domain, the NMR-structure (PDB 2LUI) (Figure 4A) (Erlendsson et al., 2014) was used. For the BAR domain dimer, we generated a homology model of the monomers by threading PICK1 residues on the crystal structure of the arfaptin-2 BAR domain. Different dimer interfaces giving rise to varying length and curvature of the BAR domain were initially tested in rigid body modeling against the SAXS data, however the interface from the arfaptin-2 crystal structure clearly gave the best result. We subsequently used molecular dynamics (MD) simulations to identify the structure of its dimeric assembly and assess the quality of the model before performing final all atom MD simulation to obtain a stable BAR domain dimer model (Figure 4B, see Figure S3, methods and SI for details). Unfortunately, oligomerization and inability for substitute endogenous cysteines hampered experimental validation of the BAR domain dimer interface by e.g. cross-linking or FRET. Finally, the N- and C-termini, as well as the linker between the PDZ domain and the BAR domain, were considered to have a random coil structure, which was supported by backbone chemical shifts from NMR experiments (see Figure 4C and S3 as well as SI for details).

Structural Analysis of PICK1^{LKV} dimers using the Ensemble Optimisation Method (EOM)

Classical Bio-SAXS approach to the data analysis (Koch et al., 2003), based on bead and/or rigid-body modeling of a single monodisperse structure to the decomposed experimental dimer form factor did not provide good or meaningful fits. This is an indirect sign of structural dispersion of the dimer structure arising from e.g. the flexible linker between the BAR and PDZ domains as well as the N- and C-termini. Consequently, to extract structural information from the SAXS data, the refinement of the dimer structure against the SAXS dimer form factor was carried out using an approach that combined rigid body modelling and EOM (SI for details) (Bernadó et al. 2007, Petoukhov, et al. 2012). A large number of potential dimeric structures were generated using the above described structural modules. The linker between the PDZ and BAR domains, as well as the N- and C-termini, were defined as flexible, whereas the PDZ domains and the BAR domain dimer were kept conformationally rigid. This yielded a population of dimers with varying positions of the PDZ domains, within the constraints given by the length of the linker and steric avoidance. The theoretical scattering from each model was calculated (with RANCH), and an ensemble of structures was optimized using the genetic algorithm (GAJOE) in EOM to fit the theoretical scattering to the SAXS data. Through this approach, a model for the PICK1^{LKV} dimer was obtained by refinement against the above described decomposed dimer form factor (Figure 5A). The wide distributions of D_{max} and R_g selected by EOM, show that the PICK1^{LKV} dimer indeed has a very flexible structure (Figure 5A). The best ensemble, containing 4 different poses, is visualized in Figure 5B.

The PDZ domains of PICK1 dimers are flexible with respect to the BAR domain

Analysis of the structural models from 100 optimized ensembles provided distributions of distances between PDZ domains (center of mass) and specific points on the BAR domain dimer (Figure 5C). The most frequent structures in the ensemble displayed distances from the PDZ domains to the attachment point on the BAR domain of 20-60 Å in (random coil ~50 Å for 40 amino acids (Tanford et al., 1966)). Moreover, the distance from the PDZ domains to the tip of the BAR domain (blue) is generally shorter than to the center of the BAR domain (green) (20-40 Å vs. 60-100 Å, respectively). The distance between PDZ domains (orange) were mostly between 120 Å and 180 Å, often representing the largest distances in the protein. To experimentally test this model, we performed cellular FRET measurements of N- and C-terminal fusion of fluorescently labeled PICK1. Whereas the N_{FRET} for PICK1-eYFP + PICK1-eCFP was significantly higher than for eYFP + eCFP (0.096 ± 0.01 vs 0.018 ± 0.01, $P<0.01$) there was no significant difference between eYFP-PICK1 + eCFP-PICK1 and eYFP + eCFP (0.024 ± 0.004 vs 0.018 ± 0.01) (n=4, one-way ANOVA with Bonferroni's post test). Indeed, this supports the EOM model suggesting that the N-terminal PDZ domain are spaced far apart. In conclusion, our findings suggest that the PDZ domains in the PICK dimer, in contrast to accessory domains in other BAR domain proteins, are separated from the BAR domain, staying far from each other and freely exploring the space around the tips of the BAR domain.

EOM investigation of the PICK1 oligomerisation mode

An EOM analysis against the experimental SAXS data clearly underlined that neither $PICK1^{WT}$ nor $PICK1^{LKV}$ could be described by an ensemble of dimers only. This prompted us to include tetramers into the EOM pool, where the conformation of the BAR-domain of the $PICK^{WT}$ was assumed similar to that determined for $PICK1^{LKV}$. By translating and rotating the BAR domain dimer, several putative tetrameric arrangements of the BAR domains were tested (Figure 6). The modes termed ‘offset’ and ‘side’ (Figure 6A and D) mimicks the BAR-BAR interactions observed for PinkBAR and the F-BAR protein FBP17/CIP4, with different extent of overlap (Frost et al., 2008; Pykalainen et al., 2011). The ‘helix’ mode (Figure 6B) mimics the BAR-BAR interaction observed for endophilin, whereas the ‘tip-tip’ interactions (Figure 6C) have been observed for endophilin, FBP17/CIP4 and PACSIN (Bai and Zheng, 2013; Frost et al., 2008; Mim et al., 2012). A hypothetical configuration resembling a circle was included as control (Figure 6E). These tetrameric arrangements were kept fixed while generating random positions of the linker regions (and consequently the PDZ domains) and the N- and C-termini, as described above for the dimeric structures.

Each tetramer pool, in combination with the dimer pool (from Figure 5), was evaluated with EOM against SAXS data of $PICK1^{LKV}$, which consisted mainly of dimers and tetramers as suggested by the biochemical data (see Figure 1). Figure 6 shows the EOM analysis of the putative modes of oligomerization for $PICK1^{LKV}$. Comparing the fits and chi-values, we found that the ‘offset’ mode provided the best fit to the data (Figure 6A). Consequently, this mode was used in the subsequent analysis. The ‘helix’ mode based on the arrangement of endophilin BAR domains on tubules (Mim et al., 2012) also yielded good fits to the experimental data, although inferior to the fits from the ‘offset’ mode (Figure 6B). On the

other hand, the ‘tip-to-tip’, side-by side’ and ‘circle’ mode produced significantly worse fits (Figure 6C-E), including systematic underestimation of the scattering intensities at low *q* region (Figure 6D-E), suggesting that these modes are too compact to fit the scattering data well.

Structural investigation and flexibility of PICK1^{LKV} tetramers

Based on the information from the dimers and the mode of oligomerisation, the structure and flexibility of the PICK1^{LKV} tetramers were investigated. EOM selected distributions of D_{max} and R_g that were narrower than for the dimer, suggesting that the tetramer is less flexible (Figure 7A). The best ensemble, again containing 4 poses, is shown in Figure 7B and the distance distributions are shown in Figure 7C. The distance distribution histograms reveal that the distal PDZ domains localize closer to the center of the BAR domain, whereas the central PDZ domains stretch out compared to the dimeric structure. The distance between PDZ domains from the same dimer (100-140 Å) (orange) is slightly shorter than the corresponding distance in the dimer model. The distance between distal PDZ domains (red) was mostly between 200 and 260 Å, indicating that the maximal distance is represented by the BAR domain tetramer (270 Å). Finally, the distance between the central PDZ domains (yellow) display a broad distribution (40-120 Å) indicating flexibility but also that they occasionally may come in contact. In conclusion, despite minor changes in the interdomain arrangements between the dimeric and tetrameric species, the PDZ domains in the tetrameric structure are also separated from the BAR domain with highly flexible interconnecting linkers.

Concentration dependence of the PICK1 oligomerization

The biochemical analysis, the model independent SAXS parameters and the EOM analysis consistently suggested concentration dependent oligomerization of PICK1. To further characterize the concentration dependence of the oligomerization process, we performed EOM analysis for the different concentrations using the dimer pool combined with the ‘offset’ mode tetramer pool. For the PICK1^{LKV} data, we observed a concentration dependent shift from predominantly dimers (at the lowest concentration), to almost exclusively tetramers (at the highest concentration) (Figure 8). Similar analysis of PICK1^{WT}, using only dimers and tetramers, allowed reasonable fits at low concentrations (up to 3.2 mg/ml), but at higher concentrations the fits systematically underestimated the scattering intensity, particularly at lower scattering angles, suggesting the presence of higher order species (Figure S4) in aggrement with the AUC experiments.

Hexamers and octamers were generated in RANCH following the same principles as for the tetramer formation by duplicating the BAR dimer. For PICK1^{WT}, the EOM did not select any structures from the hexamer pool, but included a significant octamer pool, allowing a good fit to the data (Figure 9). Since the fitting procedure at this level includes a number of random parameters, a reliable conclusion regarding the presence or absence of hexamers is not possible. Rather, it suffices to state that PICK1^{WT} has a pronounced tendency to form higher oligomers in solution, which can be fitted to our SAXS data by introducing a combination of dimers, tetramers and octamers. For PICK1^{LKV}, the inclusion of higher

oligomers in the random pools did not improve the fit (Figure S5). This confirms that there is no significant proportion of higher oligomers present in PICK1^{LKV}.

Discussion

BAR domains are membrane binding and sculpting protein modules involved in a wide variety of different cellular processes, including e.g. budding and fission during endocytosis from the plasma membrane and during production of dense core vesicles at the trans-Golgi network. The BAR domain is composed of two subunits and is believed to bind membranes as dimers. The curvature sensing capacity, as well as the scission capacity of the domains, largely reside in amphipathic helixes flanking the BAR domains (Bhatia et al., 2009; Boucrot et al., 2012) and recently a lattice-like arrangement of BAR domains on membrane tubules has been suggested to stabilize and shape tubule structure (Frost et al., 2008; Mim et al., 2012).

Higher order oligomers have also been observed in solution in absence of lipid membrane for the F-BAR domain CDC15 (Roberts-Galbraith et al., 2010), the F-BAR domain protein PACSIN1 (Halbach et al., 2007) and the I-BAR protein PinkBAR (Pykalainen et al., 2011). Here, we demonstrate that the BAR domain protein PICK1 forms higher order structures in the absence of lipids in solution at micromolar concentrations. The oligomerization was reversible and supported both by SEC and AUC. Moreover, EOM analysis of the SAXS data suggests a mix of dimers, tetramers and higher oligomers (likely octamers). The absolute distribution between the different oligomeric forms, however, is not easily compared between AUC and SAXS data, due to differences in preparation (FPLC peak 2 for AUC vs ultracentrifuged samples for SAXS), and equilibration times. Neither AUC nor EOM analysis of the SAXS data indicated any monomers in our samples suggesting high affinity for the PICK1 BAR domain dimer.

The use of EOM analysis in this study allowed us to obtain the first direct structural information on the oligomerization mode in solution for a BAR domain protein. The data can only be adequately fitted using an elongated oligomerization mode involving an offset between the individual BAR domain bearing more resemblance to the crystal structure of PinkBAR (Pykalainen et al., 2011), than the side-by-side arrangement in the crystal structure of PACSIN2 (Bai and Zheng, 2013). The resolution of the SAXS/EOM procedure does not allow us to investigate the oligomerization interface in detail, but based on the model of the BAR domain from MD simulations, we cannot identify any protruding hydrophobic residues similar to Trp141, which is important for Pinkbar oligomerization (Pykalainen et al., 2011). This lateral oligomeric assembly mode also somewhat resembles the one reported for the F-BAR domains FBP17/CIP4 on lipid tubules (Frost et al., 2008), although with a smaller overlap. The tip-to-tip interaction, seen for FBP17/CIP4, and also for endophilin A1 and PACSIN 2 on membrane tubules (Bai and Zheng, 2013; Mim et al., 2012), however, was not supported by the EOM analysis for PICK1 in solution. Although our best model suggests a direct interaction between the BAR-BAR dimers, the data are almost equally compatible with the helix-helix interaction mode observed for endophilin A1 on membrane tubules (Mim et al., 2012), in which the N-terminal amphipathic helices embedded in the membrane served as a perpendicular spacer of individual dimers. Detailed molecular insight into

interplay between membrane binding, oligomerization and folding/shielding of the amphipathic helix is likely to shed light on the functional regulation of the protein. Of note, the PDZ domains from two separate dimers are in proximity within this oligomeric arrangement, suggesting that the reported dimerization of the PICK1 PDZ domain (Pan et al., 2007) could be formed between separate dimers. The EOM analysis, however, does not support a stable PDZ-PDZ interaction.

We were unable to fit the SAXS data using classical rigid body modeling even with a number of putative dimer interfaces producing different length and curvature of the BAR domain. Consequently, we turned to EOM analysis of the PICK1^{LKV} dimer, which suggests that the PDZ domains are clearly separated from the BAR domain, and cellular FRET studies extended these findings to the WT protein in a cellular context. This is different from what has been observed for the PX/PH domains of Snx9, endophilin, and APPL1 that were all associated with the BAR domain either at the side or the tip. Such a flexible interdomain arrangement has been observed from computational studies as well (He et al., 2011), concieveably enables PICK1 to perform highly flexible scaffolding of membrane associated protein complexes and potentially flexible supramolecular scaffolding for the oligomers.

As for the auto-inhibition, it could be speculated that the C-terminal self-association in PICK1^{LVK} restricts the PDZ domain from entering the space under the BAR domain. Steric hinderance by such an interdomain arrangement has been suggested to underlie the auto-inhibition of the PICK1 BAR domain (Hanley, 2008; Lu and Ziff, 2005), and fits with the alleviation of auto-inhibition seen for PICK1^{LKV}. There is, however, no evidence of reduced flexibility of PICK1^{WT} compared to PICK1^{LKV}, and the selected dimer pools showed size and R_g distributions similar to PICK1^{LKV}. Furthermore, the PICK1^{WT} EOM analysis does not sample conformations with PDZ domains close to the BAR domain. Alternatively, the reduced cellular clustering of PICK1^{LKV} might result from tethering of the C-terminus, which has been demonstrated to counteract cellular clustering and lipid binding (Jin et al., 2006), however the low density of the unstructured C-terminus prevents us from addressing this flexibility reliably in SAXS measurements. Finally, if the oligomerization indeed involves the amphipathic helix preceeding the BAR domain, an alternative scenario is that oligomerization could directly compete with membrane interaction and consequently mediate the auto-inhibition of PICK1.

The possible relevance of our structural data was supported by cell-based experiments providing evidence based on crosslinking that PICK1 indeed forms higher order structures also in living cells. Our cellular data moreover showed a striking redistribution of eYFP-PICK1^{LKV} compared to eYFP-PICK1^{WT}. Whereas eYFP-PICK1^{WT} exhibited diffuse localization, eYFP-PICK1^{LKV} displayed massive clustering, that likely reflects enhanced membrane binding. This, together with the enhanced vesiculation capacity of eYFP-PICK1^{LKV}, supports alleviated auto-inhibition in this mutant. The clustering also suggest that the combined ability of PICK1 to bind and deform lipid membranes can lead to dramatically high local concentrations of PICK1 when unrestrained. Altogether, we therefore suggest a model where oligomerization in solution governs auto-inhibition of the BAR domain and thereby unrestrained activity, which in turn allows for specific and reversible cellular functions of PICK1 that otherwise would be impossible.

Experimental Procedures

Cloning, protein purification and biochemical characterization

WT PICK1 and PICK1-LKV were cloned and expressed in *E. coli* as described previously (Madsen 2005) (see also SI).

Cellular cross-linking

COS-7 cells were grown as described (Madsen et al., 2008) and seeded on poly ornithine coated Labtek chambers (Thermo Scientific) and transfected using Lipofectamine2000 (Invitrogen) (0.5μg DNA/300,000 cells). For crosslinking in cells, COS7 cells were transfected with pCMVmycPICK1 (Madsen et al., 2008) and grown in a 40 mm petridish. Crosslinking was performed 48 h after transfection with 1mM DSS (disuccinimidyl suberate) (Thermo Scientific) in PBS, pH 7.4 on ice for 30 minutes. The reaction was stopped by adding TBS with 1 vol% TX-100, 1 mM DTT, DNAse and protease inhibitor cocktail (Pierce). Cell lysates were analyzed by 10% SDS-PAGE followed by western blotting using rabbit αPICK1 ab (Abcam).

Liposome vesiculation assay

The vesiculation capacity was measured as modified from (Boucrot et al., 2012). Liposomes produced from Folch brain liposomes and 1% fluorescently conjugated lipid DiD (1,1′-Dioctadecyl - 3,3,3′,3′-tetramethylindodicarbocyanine iodide) were extruded through 200 nm filters at a ‘concentration’ of 0.25 mg/ml and incubated with 10 μM protein for 1 h, before spinning at 200,000 × G for 15 minutes in a final buffer of TBS + 0.0025 vol% TX-100 + 0.25 mM DTT. Supernatants were collected immediately and pellet was resuspended in buffer. Vesiculation was measured in the supernatants as the absorbance at 648 nm reflecting the amount of DiD present and thereby the degree of liposome disruption.

Molecular modeling and dynamics simulation

A molecular model of the PICK1-BAR domain monomer was built with homology modeling using arfaptin 2 as a template (PDB ID: 1I49). This model was used in extensive coarse-grained (CG) molecular dynamics (MD) simulations to determine the structure of its dimeric assembly (See also SI). Additionally, three alternative models for the PICK1-BAR dimers were constructed with homology modeling using, arfaptin, amphiphysin and endophilin BAR dimers as templates. The relative quality of these three models together with the best dimer model obtained from the CG-MD (CG-model) was assessed with all-atom (AA) MD simulations (See also SI) using several different criteria, such as their stability (RMSD), solvent-accessible surface area (SASA) of hydrophobic residues, and surface area of hydrophobic residues buried in the dimer interface. The CG-model performed best and was further equilibrated in subsequent AA-MD and used as our final model of the PICK1-BAR dimer (see SI for details).

SAXS data acquisition and analysis

Acquisition—The scattering experiments were carried out at the EMBL X33 beamline (C. E. Blanchet, 2012) at the DORIS storage ring (DESY, Hamburg) following standard procedures (see also SI).

Ensemble Optimization Method (EOM)

Populations of 10.000 structures each were generated with Ranch (Bernado et al., 2007; Petoukhov and Svergun, 2012). Scattering curves were calculated for each structure from [0.0001 to 0.5Å^{-1}] using 15 spherical harmonics. Optimal ensembles were fitted to experimental data with the program Gajoe (Bernado et al., 2007; Petoukhov and Svergun, 2012), with 2000 generations and 100 repeats (see also SI).

Analytical decomposition of SAXS data

The small-angle scattering from oligomers, in the absence of structure factors, are simply the sum the scattering from the single components: This implies that the scattering from two samples with different fractions of the same two components, can be decomposed to obtain the form factors of the single components by solving two equations with two unknowns. This is exploited in order to determine the solution structure of the dimer and the tetramer (see also SI).

Supplementary Material

Refer to Web version on PubMed Central for supplementary material.

Acknowledgments

The work was supported by the National Institute of Health Grants P01 DA 12408 (UG), the Danish Medical Research Council (UG, BV), University of Copenhagen BioScaRT Program of Excellence (UG, KLM), the Lundbeck Foundation Center for Biomembranes in Nanomedicine (UG,), the Drug Research Academy (XT), Novo Nordisk A/S (XT), DANSCATT (MLC, LA) and the UNIK Center for Synthetic Biology (UG, MLC, KLM). Computational resources of XSEDE, and of the David A. Cofrin Center for Biomedical Information in the HRH Prince Alwaleed Bin Talal Bin Abdulaziz Alsaud Institute for Computational Biomedicine are gratefully acknowledged.

Biography

Karlsen et al. present structures of PICK1 demonstrating that the protein-binding PDZ domains are flexible with respect to the membrane binding BAR domain enabling long range scaffolding interactions. Furthermore, PICK1 oligomerization involves an offset, parallel arrangement of the BAR domains, possibly governing BAR domain auto-inhibition.

References

Anggono V, Huganir RL. Regulation of AMPA receptor trafficking and synaptic plasticity. Curr Opin Neurobiol. 2012

Bai X, Zheng X. Tip-to-tip interaction in the crystal packing of PACSIN 2 is important in regulating tubulation activity. Protein Cell. 2013

Bernado P, Mylonas E, Petoukhov MV, Blackledge M, Svergun DI. Structural characterization of flexible proteins using small-angle X-ray scattering. J Am Chem Soc. 2007; 129:5656–5664. [PubMed: 17411046]

Bhatia VK, Madsen KL, Bolinger PY, Kunding A, Hedegard P, Gether U, Stamou D. Amphipathic motifs in BAR domains are essential for membrane curvature sensing. The EMBO journal. 2009; 28:3303–3314. [PubMed: 19816406]

Boucrot E, Pick A, Camdere G, Liska N, Evergren E, McMahon HT, Kozlov MM. Membrane fission is promoted by insertion of amphipathic helices and is restricted by crescent BAR domains. Cell. 2012; 149:124–136. [PubMed: 22464325]

Blanchet CE, A.V.Z. Kikhney AG, Franke D, Konarev PV, Shang W, Klaering R, Ro brahn B, Hermes C, Cipriani F, Svergun DI, Roessle M. Instrumental setup for high-throughput small-and wide-angle solution scattering at the X33 beamline of EMBL Hamburg. Journal of Applied Crystallography. 2012; 45

Cao M, Mao Z, Kam C, Xiao N, Cao X, Shen C, Cheng KK, Xu A, Lee KM, Jiang L, et al. PICK1 and ICA69 control insulin granule trafficking and their deficiencies lead to impaired glucose tolerance. PLoS biology. 2013; 11:e1001541. [PubMed: 23630453]

Cao M, Xu J, Shen C, Kam C, Huganir RL, Xia J. PICK1-ICA69 heteromeric BAR domain complex regulates synaptic targeting and surface expression of AMPA receptors. The Journal of neuroscience : the official journal of the Society for Neuroscience. 2007; 27:12945–12956. [PubMed: 18032668]

Citri A, Bhattacharyya S, Ma C, Morishita W, Fang S, Rizo J, Malenka RC. Calcium binding to PICK1 is essential for the intracellular retention of AMPA receptors underlying long-term depression. The Journal of neuroscience : the official journal of the Society for Neuroscience. 2010; 30:16437–16452. [PubMed: 21147983]

Elkins JM, Papagrigoriou E, Berridge G, Yang X, Phillips C, Gileadi C, Savitsky P, Doyle DA. Structure of PICK1 and other PDZ domains obtained with the help of self-binding C-terminal extensions. Protein Sci. 2007; 16:683–694. [PubMed: 17384233]

Erlendsson S, Rathje M, Heidarsson PO, Poulsen FM, Madsen KL, Teilum K, Gether U. PICK1 (protein interacting with C-kinase 1) binding promiscuity relies on unconventional PDZ (PSD-95/Discs-large/ZO-1 homology) binding modes for non-class II PDZ ligands. The Journal of biological chemistry. 2014

Frost A, Perera R, Roux A, Spasov K, Destaing O, Egelman EH, De CP, Unger VM. Structural basis of membrane invagination by F-BAR domains. Cell. 2008; 132:807–817. [PubMed: 18329367]

Glatter. O. new method for the evaluation of small-angle scattering data. Journal of Applied Crystallography. 1977:10.

Halbach A, Morgelin M, Baumgarten M, Milbrandt M, Paulsson M, Plomann M. PACSIN 1 forms tetramers via its N-terminal F-BAR domain. FEBS J. 2007; 274:773–782. [PubMed: 17288557]

Hanley JG. PICK1: a multi-talented modulator of AMPA receptor trafficking. Pharmacol Ther. 2008; 118:152–160. [PubMed: 18353440]

He Y, Liwo A, Weinstein H, Scheraga HA. PDZ binding to the BAR domain of PICK1 is elucidated by coarse-grained molecular dynamics. Journal of molecular biology. 2011; 405:298–314. [PubMed: 21050858]

Holst B, Madsen KL, Jansen AM, Jin C, Rickhag M, Lund VK, Jensen M, Bhatia V, Sorensen G, Madsen AN, et al. PICK1 deficiency impairs secretory vesicle biogenesis and leads to growth retardation and decreased glucose tolerance. PLoS biology. 2013; 11:e1001542. [PubMed: 23630454]

Jansen AM, Nassel DR, Madsen KL, Jung AG, Gether U, Kjaerulff O. PICK1 expression in the Drosophila central nervous system primarily occurs in the neuroendocrine system. J Comp Neurol. 2009; 517:313–332. [PubMed: 19757495]

Jin W, Ge WP, Xu J, Cao M, Peng L, Yung W, Liao D, Duan S, Zhang M, Xia J. Lipid binding regulates synaptic targeting of PICK1, AMPA receptor trafficking, and synaptic plasticity. Journal of Neuroscience. 2006; 26:2380–2390. [PubMed: 16510715]

Koch MH, Vachette P, Svergun DI. Small-angle scattering: a view on the properties, structures and structural changes of biological macromolecules in solution. Quarterly reviews of biophysics. 2003; 36:147–227. [PubMed: 14686102]

Li J, Mao X, Dong LQ, Liu F, Tong L. Crystal structures of the BAR-PH and PTB domains of human APPL1. Structure. 2007; 15:525–533. [PubMed: 17502098]

Lu W, Ziff EB. PICK1 interacts with ABP/GRIP to regulate AMPA receptor trafficking. Neuron. 2005; 47:407–421. [PubMed: 16055064]

Madsen KL, Beuming T, Niv MY, Chang CW, Dev KK, Weinstein H, Gether U. Molecular determinants for the complex binding specificity of the PDZ domain in PICK1. Journal of Biological Chemistry. 2005; 280:20539–20548. [PubMed: 15774468]

Madsen KL, Eriksen J, Milan-Lobo L, Han DS, Niv MY, mmendrup-Johnsen I, Henriksen U, Bhatia VK, Stamou D, Sitte HH, et al. Membrane localization is critical for activation of the PICK1 BAR domain. Traffic. 2008; 9:1327–1343. [PubMed: 18466293]

Madsen KL, Thorsen TS, Rahbek-Clemmensen T, Eriksen J, Gether U. Protein Interacting with C Kinase 1 (PICK1) Reduces Reinsertion Rates of Interaction Partners Sorted to Rab11-dependent Slow Recycling Pathway. The Journal of biological chemistry. 2012; 287:12293–12308. [PubMed: 22303009]

Meinecke M, Boucrot E, Camdere G, Hon WC, Mittal R, McMahon HT. Cooperative recruitment of dynamin and BIN/amphiphysin/Rvs (BAR) domain-containing proteins leads to GTP-dependent membrane scission. J Biol Chem. 2013; 288:6651–6661. [PubMed: 23297414]

Mim C, Cui H, Gawronski-Salerno JA, Frost A, Lyman E, Voth GA, Unger VM. Structural basis of membrane bending by the N-BAR protein endophilin. Cell. 2012; 149:137–145. [PubMed: 22464326]

Pan L, Wu H, Shen C, Shi Y, Jin W, Xia J, Zhang M. Clustering and synaptic targeting of PICK1 requires direct interaction between the PDZ domain and lipid membranes. The EMBO journal. 2007; 26:4576–4587. [PubMed: 17914463]

Pedersen JS, Hansen S, Bauer R. The aggregation behavior of zinc-free insulin studied by small-angle neutron scattering. Eur Biophys J. 1994; 22:379–389. [PubMed: 8149922]

Perez JL, Khatri L, Chang C, Srivastava S, Osten P, Ziff EB. PICK1 Targets Activated Protein Kinase C{alpha} to AMPA Receptor Clusters in Spines of Hippocampal Neurons and Reduces Surface Levels of the AMPA-Type Glutamate Receptor Subunit 2. Journal of Neuroscience. 2001; 21:5417–5428. [PubMed: 11466413]

Petoukhov MV, Svergun DI. Applications of small-angle X-ray scattering to biomacromolecular solutions. Int J Biochem Cell Biol. 2012; 45:429–437. [PubMed: 23142499]

Pykalainen A, Boczkowska M, Zhao H, Saarikangas J, Rebowski G, Jansen M, Hakanen J, Koskela EV, Peranen J, Vihinen H, et al. Pinkbar is an epithelial-specific BAR domain protein that generates planar membrane structures. Nature structural & molecular biology. 2011; 18:902–907.

Pylypenko O, Lundmark R, Rasmuson E, Carlsson SR, Rak A. The PX-BAR membrane-remodeling unit of sorting nexin 9. EMBO J. 2007; 26:4788–4800. [PubMed: 17948057]

Rao Y, Ma Q, Vahedi-Faridi A, Sundborger A, Pechstein A, Puchkov D, Luo L, Shupliakov O, Saenger W, Haucke V. Molecular basis for SH3 domain regulation of F-BAR-mediated membrane deformation. Proc Natl Acad Sci U S A. 2010; 107:8213–8218. [PubMed: 20404169]

Roberts-Galbraith RH, Ohi MD, Ballif BA, Chen JS, McLeod I, McDonald WH, Gygi SP, Yates JR 3rd, Gould KL. Dephosphorylation of F-BAR protein Cdc15 modulates its conformation and stimulates its scaffolding activity at the cell division site. Molecular cell. 2010; 39:86–99. [PubMed: 20603077]

Rocca DL, Martin S, Jenkins EL, Hanley JG. Inhibition of Arp2/3-mediated actin polymerization by PICK1 regulates neuronal morphology and AMPA receptor endocytosis. Nature cell biology. 2008; 10:259–271. [PubMed: 18297063]

Sogaard R, Borre L, Braunstein TH, Madsen KL, MacAulay N. Functional modulation of the glutamate transporter variant GLT1b by the PDZ domain protein PICK1. The Journal of biological chemistry. 2013; 288:20195–20207. [PubMed: 23697999]

Staudinger J, Lu J, Olson EN. Specific interaction of the PDZ domain protein PICK1 with the COOH terminus of protein kinase C-alpha. Journal of Biological Chemistry. 1997; 272:32019–32024. [PubMed: 9405395]

Staudinger J, Zhou J, Burgess R, Elleedge SJ, Olson EN. PICK1: A Perinuclear Binding Protein and Substrate for Protein Kinase C Isolated by the Yeast Two-hybrid System. Journal of Cell Biology. 1995; 128:263–271. [PubMed: 7844141]

Steinberg JP, Takamiya K, Shen Y, Xia J, Rubio ME, Yu S, Jin W, Thomas GM, Linden DJ, Huganir RL. Targeted in vivo mutations of the AMPA receptor subunit GluR2 and its interacting protein PICK1 eliminate cerebellar long-term depression. Neuron. 2006; 49:845–860. [PubMed: 16543133]

Tanford C, Kawahara K, Lapanje S. Proteins in 6-M guanidine hydrochloride. Demonstration of random coil behavior. The Journal of biological chemistry. 1966; 241:1921–1923. [PubMed: 5947952]

Wang Q, Kaan HY, Hooda RN, Goh SL, Sondermann H. Structure and plasticity of Endophilin and Sorting Nexin 9. Structure. 2008; 16:1574–1587. [PubMed: 18940612]

Xia J, Zhang X, Staudinger J, Huganir RL. Clustering of AMPA receptors by the synaptic PDZ domain-containing protein PICK1. Neuron. 1999; 22:179–187. [PubMed: 10027300]

Xu J, Xia J. Structure and function of PICK1. Neurosignals. 2006; 15:190–201. [PubMed: 17215589]

Zhu G, Chen J, Liu J, Brunzelle JS, Huang B, Wakeham N, Terzyan S, Li X, Rao Z, Li G, et al. Structure of the APPL1 BAR-PH domain and characterization of its interaction with Rab5. EMBO J. 2007; 26:3484–3493. [PubMed: 17581628]

Highlights

The PDZ domains are far apart and flexible with respect to the BAR domain.

PICK1 forms higher oligomeric species in solution.

The N-BAR domain is directly involved in the parallel, offset oligomerization mode.

Oligomerization is likely to regulate BAR domain auto-inhibition.

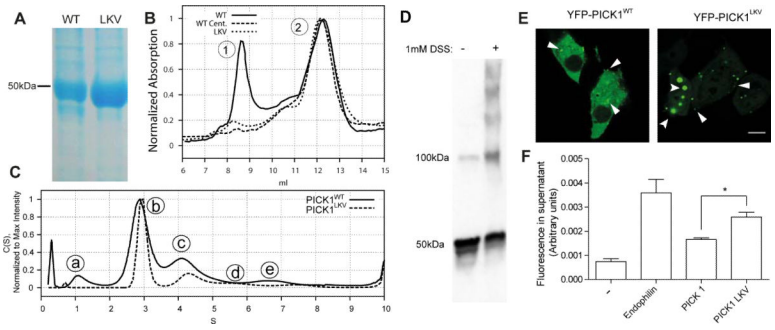

Figure 1. PICK1 exists in multiple oligomeric states and oligomerization is reduced in the self-binding mutant PICK1^{LKV}

(A) Representative SDS-PAGE (n=5) showing PICK1^{WT} (left) and PICK1^{LKV} (right). PICK1^{WT} elutes at 46 kD (monomer). A weak putative degradation product is also seen. PICK1^{LKV} displays only a band at 46 kD. (B) Size exclusion chromatography (SEC) of PICK1^{WT} (solid line), ultracentrifuged PICK1^{WT} (dashed line) and PICK1^{LKV} (dotted line). PICK1^{WT} (solid line) shows two major peaks. Peak 1 is removed by ultracentrifugation and is almost absent in PICK1^{LKV}. (C) Analytical ultracentrifugation (AUC) of fractions corresponding to peak 2 in the SEC. PICK1^{WT} (solid line) displays distinct peaks. PICK1^{LKV} displays reduced size of peaks corresponding to larger sizes. (D) Representative western blot showing lysates from COS7 cells transiently expressing PICK1^{WT} with or without pretreatment with the membrane permeable crosslinking agent DSS (n=3) (E) Representative confocal micrographs showing YFP-PICK1^{WT} (left) and YFP-PICK1^{LKV} (right) transiently expressed in COS7 cells (n=3). Arrows indicate clusters. Scale bar 10 μM. (F) Quantification of liposome vesiculation capacity of endophilin, PICK1^{WT} and PICK1^{LKV} in arbitrary units. Fluorescently labeled liposomes were incubated with indicated proteins before ultracentrifugation. Fluorescent lipids in the supernatant indicate scission from liposomes, which are pelleted (means ± sem, n=3, *$p < 0.05$). See also Figure S1.

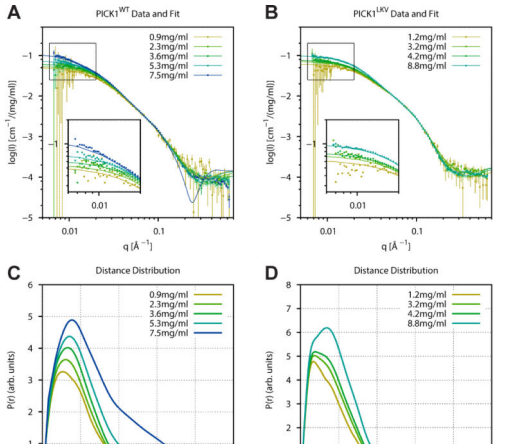

PICK1^{WT}

ID	Conc. [mg/ml]	Dmax [Å]	Rg [Å]	I0 [cm^{-1}/(mg/ml)×10^{-2}]	MM [kD]	Olig. Coef.	χ^2
wt31	1.0	250	69.66 ± 0.88	4.86 ± 0.68	73.19	1.59	2.96
wt13	2.3	230	69.57 ± 0.34	5.68 ± 0.45	85.48	1.86	1.51
wt11	3.6	230	70.38 ± 0.16	6.25 ± 0.21	94.09	2.05	2.19
wt28	5.3	270	78.54 ± 0.49	7.39 ± 0.55	111.34	2.42	2.72
wt25	7.5	480	127.59 ± 1.26	12.25 ± 1.79	184.60	4.01	4.35

PICK1^{LKV}

ID	Conc. [mg/ml]	Dmax [Å]	Rg [Å]	I0 [cm^{-1}/(mg/ml)×10^{-2}]	MM [kD]	Olig. Coef.	χ^2
L40	1.2	180	57.80 ± 0.23	5.97 ± 0.41	89.96	1.96	3.01
L20	3.2	220	64.83 ± 0.31	7.42 ± 0.42	111.71	2.43	3.86
L38	4.2	230	66.55 ± 0.24	7.98 ± 0.33	120.18	2.61	2.72
L36	8.8	250	72.34 ± 0.21	10.24 ± 0.36	154.33	3.35	4.52

Figure 2. Small-angle X-ray scattering (SAXS) experiments demonstrated concentration dependent oligomerization PICK1^{WT} and PICK1^{LKV}

Experimental SAXS data measured on five concentrations of PICK1^{WT} ranging from 0.9 - 7.5 mg/ml (A), and four concentrations of PICK1^{LKV} ranging from 1.2 - 8.8 mg/ml (B), scaled by concentration and on absolute scale. C-D) Pair distance distribution functions, *p(r)*, calculated by IFT of data shown in A and B, respectively. (Tables) Model-independent parameters derived by IFT, i.e. maximal internal distance, D_{max}, Radius of Gyration, R_g and forward scattering, *I(0)*. Note the concentration dependent shift to larger D_{max} values. See also Figure S2.

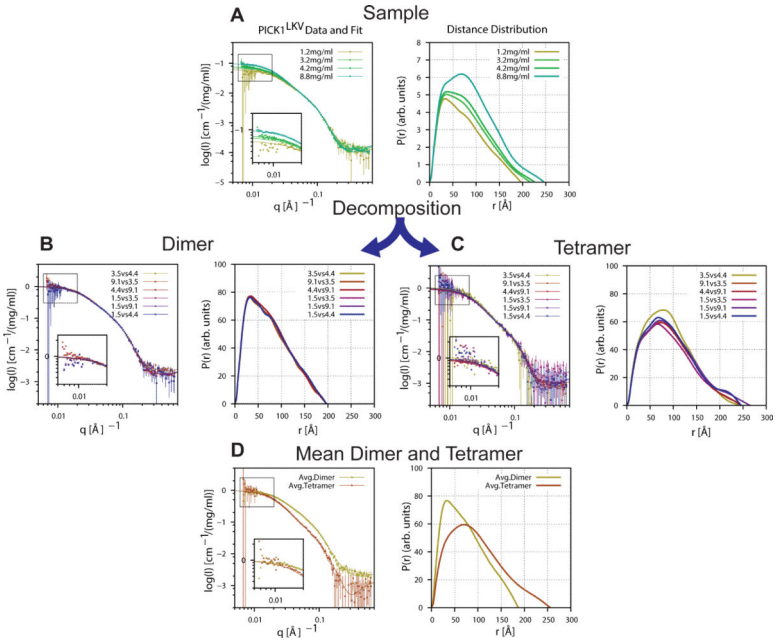

Figure 3. Decomposition of polydisperse PICK1^{LKV} SAXS data into dimer and tetramer scattering signals

(A) Concentration series of PICK1^{LKV} (same as Figure 2B and D). Left: SAXS data. Right: corresponding *p(r)* functions. (B) Six dimer SAXS form factors (left) and corresponding *p(r)* functions (right) resulting from decomposition through pairwise combination of samples at different concentrations. (C) Six tetramer SAXS form factors (left) and *p(r)* functions (right). (D) Direct comparison of the mean dimer and tetramer form factors and *p(r)* functions. Model-independent parameters are listed in Table S1.

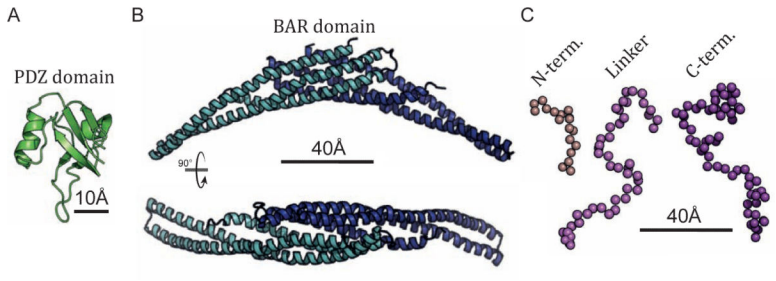

Figure 4. Structural modules in PICK1

(A) PDZ domain of PICK1 from NMR structure (PDB 2LUI) (Erlendsson et al., 2014). (B) Side and top view of the PICK1 BAR domain modeled by AA-MD simulation based on the crystal structure of the homologous Arfaptin 2. (C) Representative structures of the unstructured N-terminus, the linker between the PDZ and BAR domain, and the C-terminus. See also Figure S3.

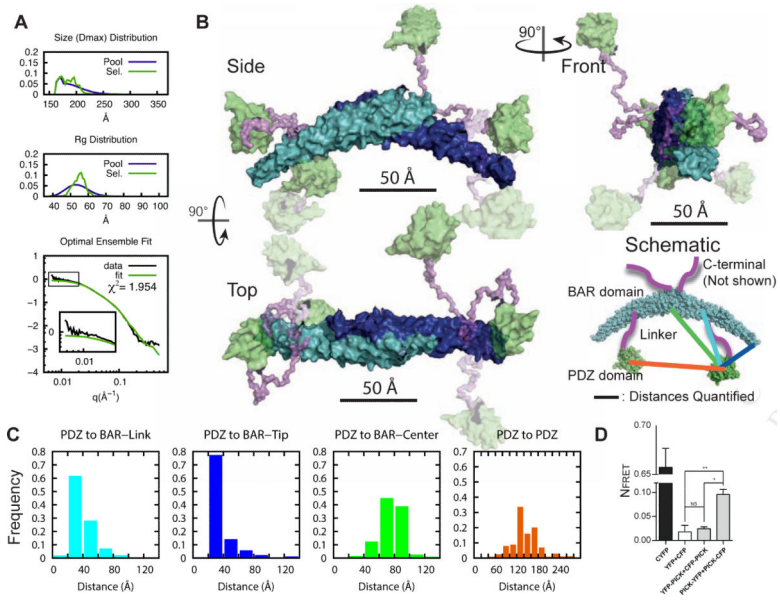

Figure 5. Interdomain arrangement in PICK1^{LKV} dimer

(A) EOM on decomposed dimer form factor of PICK1^{LKV}. Fit of optimal ensemble to combination of PICK1^{LKV} samples at 2.3 and 3.5 mg/ml. Top panels show D_{max} and middle panel R_g of generated pools in blue and selected pools in green. Bottom panel shows fit to SAXS form factor. (B) Illustration of flexibility of PICK1^{LKV}. The rigid BAR domain is shown in cyan/blue. The PDZ domain is green. Transparency reflects frequency of the conformation in the optimal ensemble. The linker region is in purple. The C-terminal is removed for visual clarity. (C) Histograms of sampled distances between the PDZ domain and the position of the linker on the BAR domain (cyan), the tip of the BAR domain (blue), and the center of the BAR domain (green), and between the PDZ domains (orange) (100 ensembles, bin size 20 Å). (D) Quantification of cellular FRET of N- and C-terminal fusions of PICK1. CFP-YFP is a direct fusion of the two fluorescent proteins. Means ± sem, n=4, *p < 0.05, **p < 0.01.

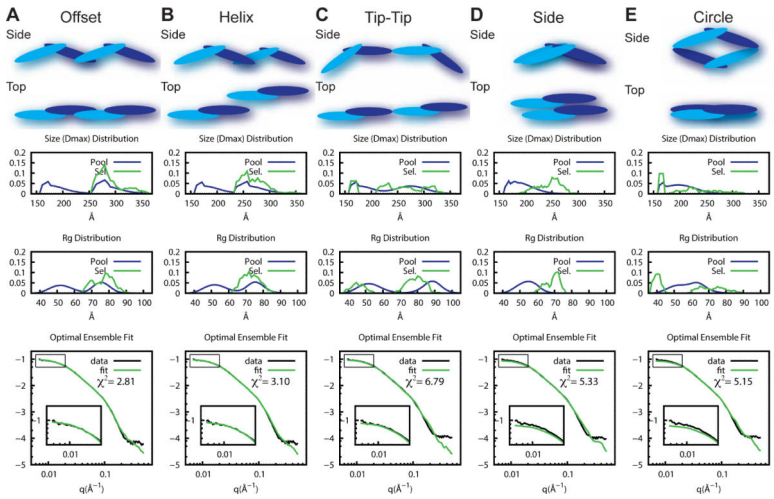

Figure 6. Dimers of dimers of PICK1^{LKV} via an 'offset' BAR-BAR arrangement

EOM fitting of five putative tetrameric structures [(A) off-set, (B) helix, (C) tip-tip, (D) side and (E) circle] to PICK1^{LKV} SAXS data at 8.8 mg/ml. Dimers are included in the analysis. Middle panels show D_{max} and R_g distributions of the randomly generated pools (blue) and selected pools (green) by EOM. Bottom panels show SAXS data and fit of the optimal ensemble. χ^2-values for the fits are shown.

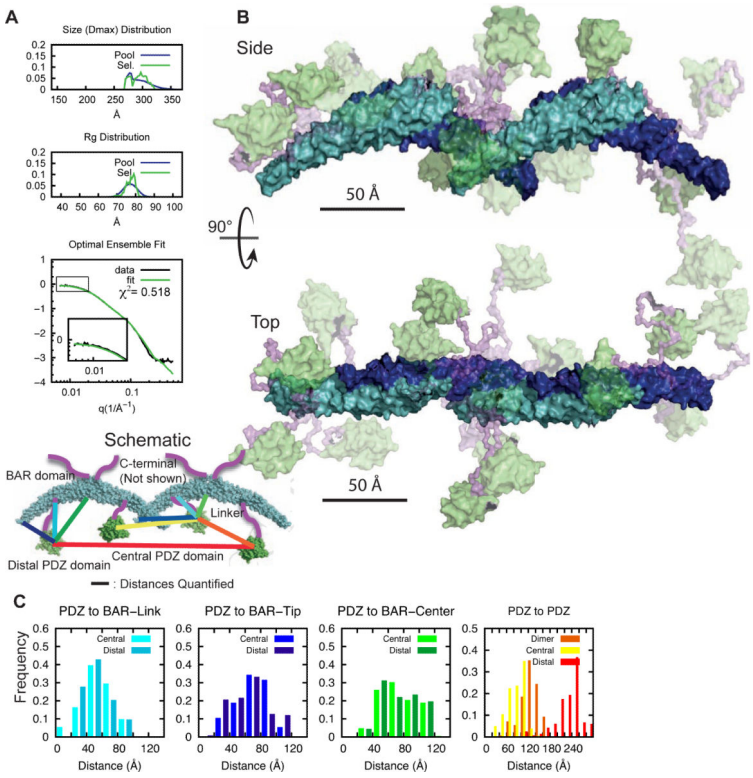

Figure 7. Interdomain arrangement in PICK1^{LKV} tetramer

(A) EOM on decomposed tetramer form factor of PICK1^{LKV}. Fit of optimal ensemble to combination of PICK1^{LKV} samples at 2.3 and 3.5 mg/ml. Top panels show D_{max} and middle panel R_g of generated pools in blue and selected pools in green. Bottom panel shows fit to SAXS form factor. (B) Illustration of flexibility of PICK1^{LKV}. The BAR domain is shown in cyan/blue. PDZ domain is green and the transparency reflects frequency of conformation in optimal ensemble. Linker region is in purple. The C-terminal is removed for visual clarity. (C) Histograms of sampled distances between the PDZ domain and the position of the linker on the BAR domain (light blues), the tip of the BAR domain (dark blues), and the center of the BAR domain (greens) and between the PDZ domains within the dimer (orange), as well as between the two distal PDZ domains (red) and the central PDZ domains (yellow) (100 ensembles, bin size 20 Å).

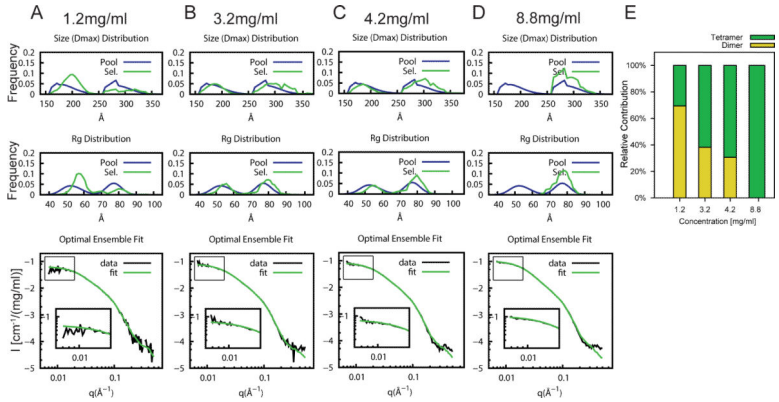

Figure 8. Concentration dependent tetramerization of PICK1^{LKV}

EOM on PICK1^{LKV} at increasing protein concentrations; (A) 1.2 mg/ml, (B) 3.2 mg/ml, (C) 4.2 mg/ml, and (D) 8.8 mg/ml. Top panels and middle panels show D_{max} and R_g of the generated pools in blue and selected pools in green. Left pool (160-230 Å) represents dimers, right pool (260-340 Å) represent tetramers. Bottom panels show SAXS data and fit of optimal ensemble. (E) Quantification of the fraction of dimers and tetramers at different concentrations of PICK1^{LKV}. For analysis of PICK1^{WT} with dimers and tetramers see Figure S4.

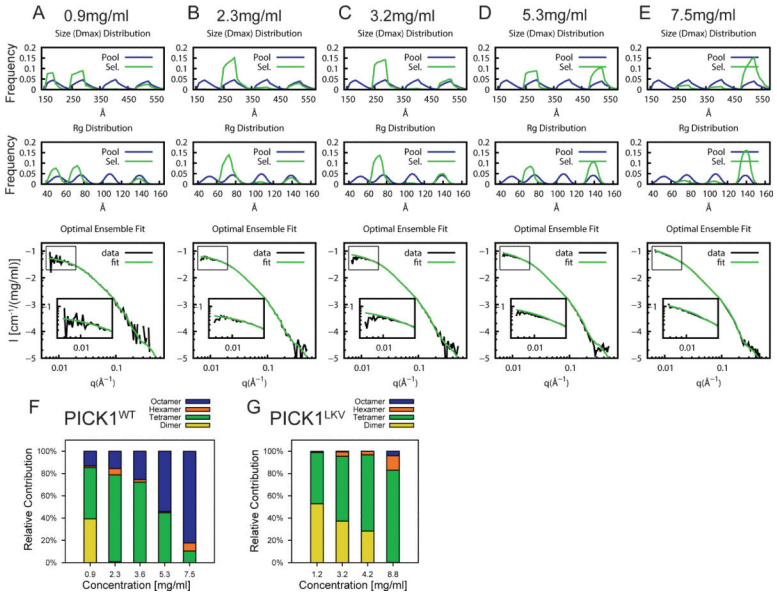

Figure 9. Concentration dependent oligomerization of PICK1^{WT}

EOM on PICK1^{WT} at increasing protein concentrations; (A) 0.9 mg/ml (B) 2.3 mg/ml (C) 3.2 mg/ml (D) 5.3 mg/ml and (E) 7.5 mg/ml, including dimers, tetramers, hexamers and octamers in the generated pool. Top panels show D_{max} and R_g of generated pools in blue and selected pools in green. Bottom panels show SAXS data and fit of optimal ensemble. (F) Quantification of the fraction of dimers, tetramers, hexamers and octamers at different concentrations of PICK1^{WT}. (G) Quantification of the fraction of dimers, tetramers, hexamers and octamers at different concentrations of PICK1^{LKV} from analysis repeated with all species (see Figure S5 for analysis).